

Chloride-Improved Crystallization in Sequentially Vacuum-Deposited Perovskites for p-i-n Perovskite Solar Cells

Supporting information

Jin Yan^{1,2}, Jasmeen Nespoli², Reinder K. Boekhoff^{1,2}, Haoxu Wang¹, Timo Gort², Martijn Tijssen¹, Bernardus Zijlstra¹, Arjan Houtepen², Tom J. Savenije², Olindo Isabella¹, Luana Mazzarella¹

1 PVMD group, Delft University of Technology, Mekelweg 4, 2628 CD Delft, the Netherlands

2 Department of ChemE, Delft University of Technology, Van der Maasweg 9, 2629 HZ Delft, the Netherlands

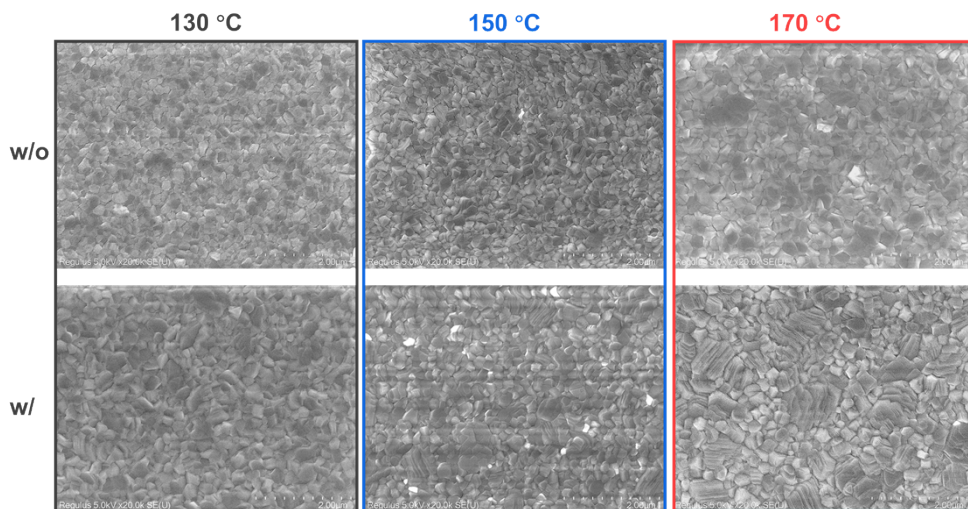


Figure S1 Top-view SEM of samples *w/o* and *w/* PbCl₂ annealed at different temperatures.

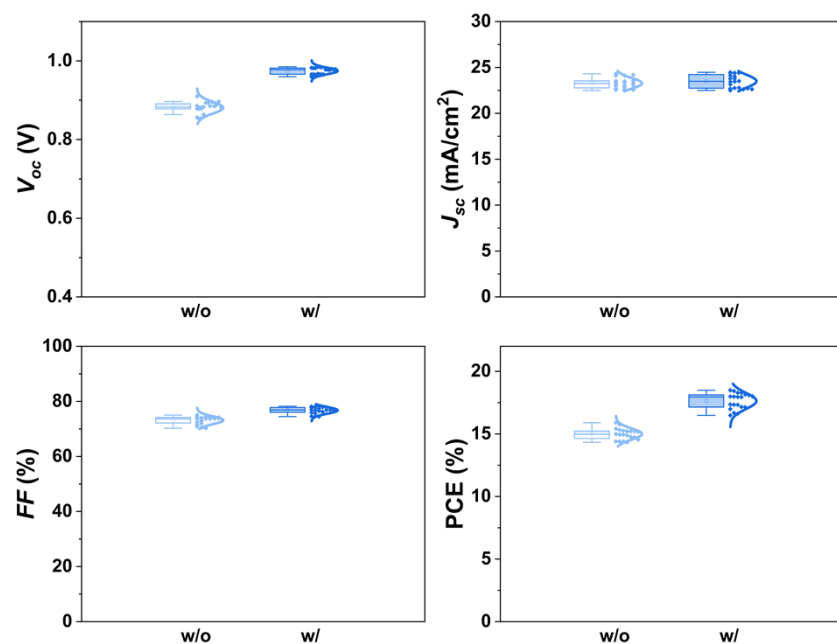


Figure S2 Statistical distribution of the photovoltaic parameters (V_{oc} , J_{sc} , FF, and PCE) of solar cells *w/* and *w/o*

PbCl_2 . Each condition includes 20 solar cells. All the samples were annealed with 150°C for 20 mins.

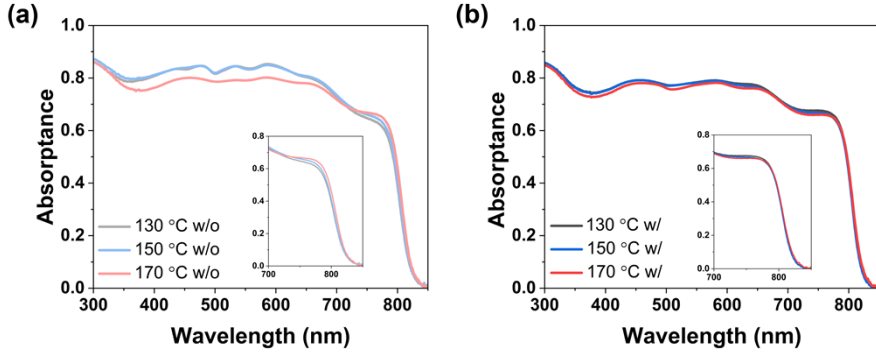


Figure S3 Absorptance spectra of samples (a) *w/o* and (b) *w/* PbCl_2 annealed at different temperatures. The inset figures zoom-in the spectra in the wavelength range of 700–850 nm.

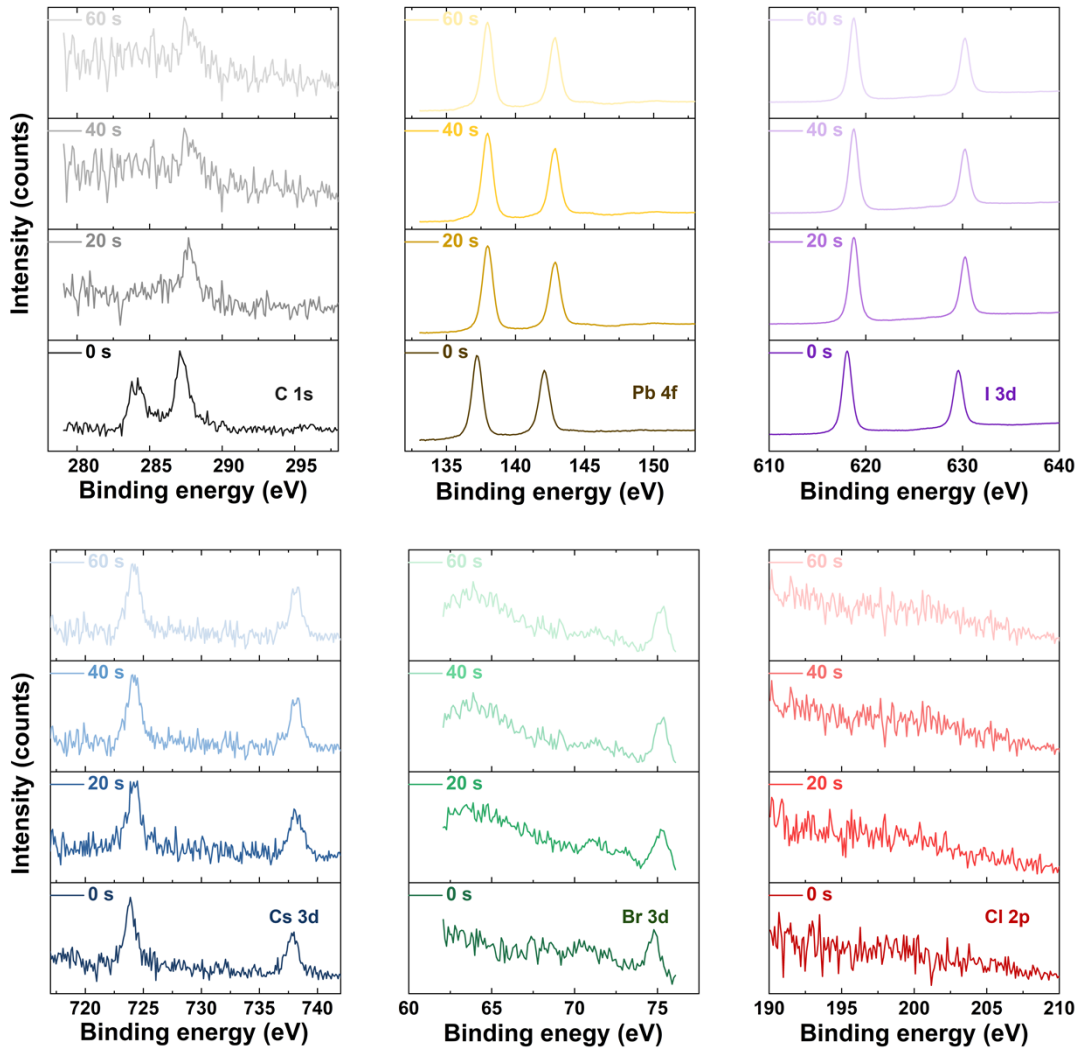


Figure S4 Fine XPS images of C 1s, Pb 4f, I 3d, Cs 3d, Br 3d, and Cl 2p peaks with different etching time (in-depth).

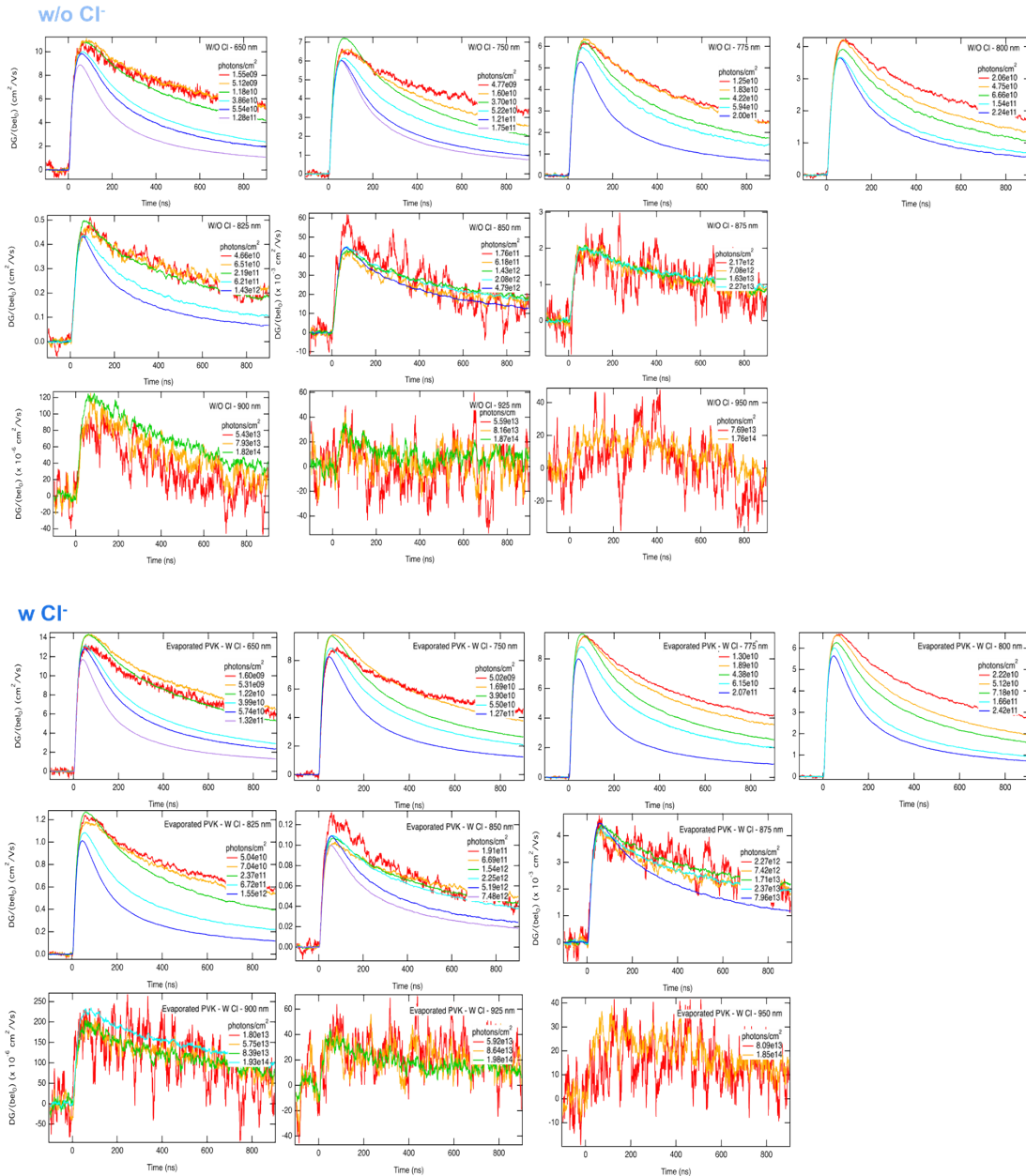


Figure S5 TRMC plots of both *w/o* and *w/* PbCl₂ samples measured with different excitation wavelength and photon intensity.

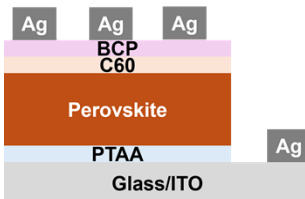


Figure S6 Schematic structure of the solar cell.

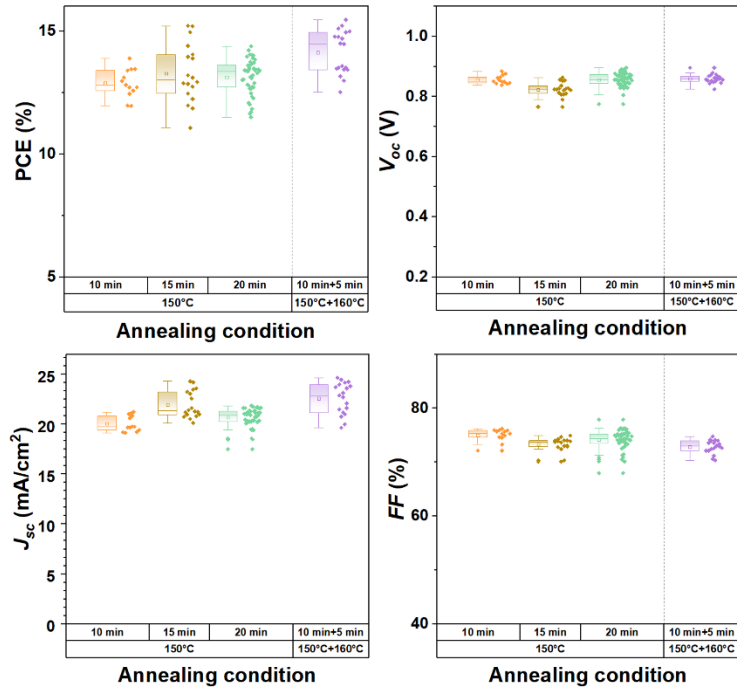


Figure S7 Statistical distribution of PSCs w/o PbCl_2 based on different annealing temperature and time. The purple distribution boxes mean that the related samples were annealed at 150 °C for 10 mins and afterwards at 160 °C for 5 mins.

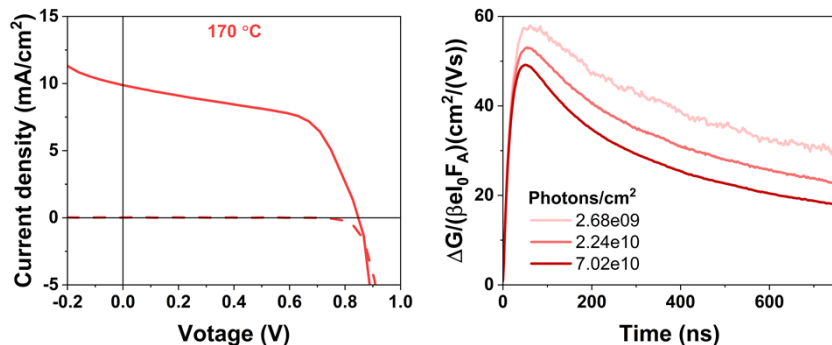


Figure S8 J - V curve of the cell and TRMC of the PVK films with 170 °C annealing for 10 mins.

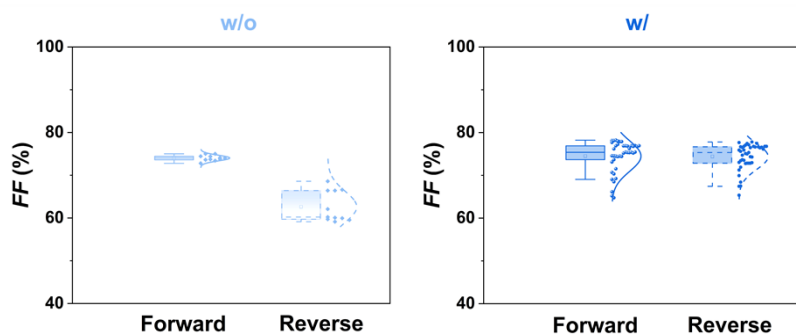


Figure S9 Statistical distribution of FF in forward and reverse scan modes of the samples (left) w/o and (right) w/ PbCl_2 .



Figure S10 Photo of degraded samples (quartz/PVK) state in ambient air.

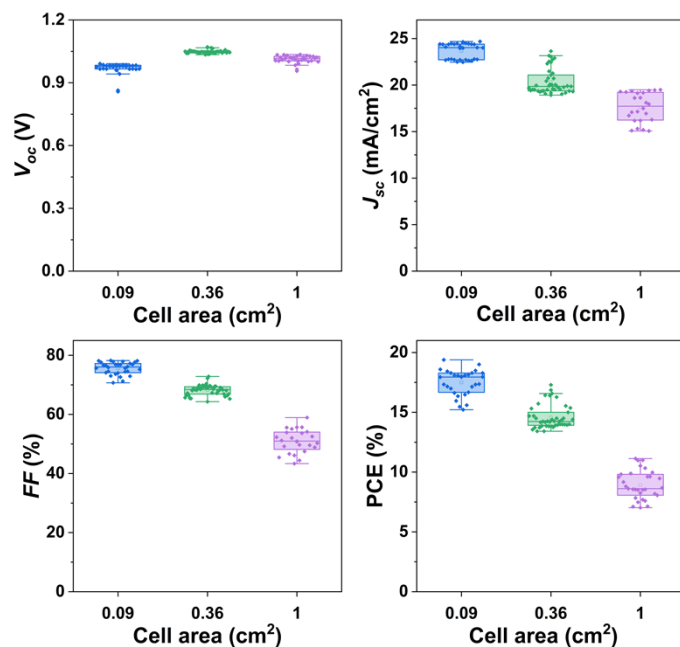


Figure S11 Distribution of external parameters (PCE, V_{oc} , J_{sc} , and FF) of PSCs as a function of cell area based on annealing condition of 150 °C and 10 mins. Data of more than 20 cells are collected for each variation. The cells of 0.09 cm² and 0.36 cm² reported here are prepared in the same batch, while the 1 cm² cells are prepared in another batch with the same deposition parameters.

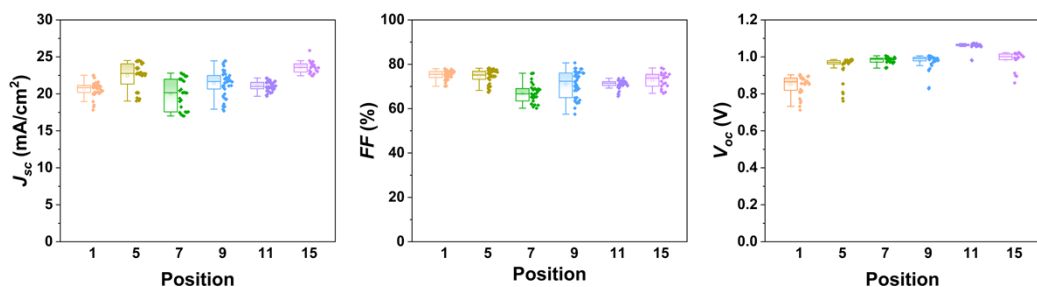


Figure S12 Statistical distribution of the V_{oc} , J_{sc} , and FF based on the samples at different position shown in **Figure 5d**.

Table S1 Processing parameters for different precursors.

Samples	PbI ₂	FAI	Precursors	CsBr	PbCl ₂
Temperature (°C)	202-236	160-180		310-330	150-170
Rate (Å/s)	1.8-2.0	1.8-2.4		0.08-0.10	0.08-0.15
Vacuum (mbar)	10 ⁻⁶ -10 ⁻⁷	10 ⁻⁶ -10 ⁻⁷		10 ⁻⁶ -10 ⁻⁷	10 ⁻⁶ -10 ⁻⁷

Table S2 Peak position of (100) for samples w/o and w/ PbCl₂ annealed at different temperature from **Figure 1b**.

Annealing temperature	w/o PbCl ₂	w/ PbCl ₂
130	13.927	13.889
150	13.891	13.885
170	13.878	13.871

Table S3 Grain size statistics obtained from top-view SEM and crystallite size calculated using the Scherrer equation.

Sample	Top-view SEM grain size	D (nm)
	(nm)	
w/ 130 °C	157	139.6
w/ 150 °C	225	170.3
w/ 170 °C	281	209.5

Table S4 Summary of best p-i-n PSCs based on sequential and co-thermally deposited absorber layer. PCE together with deposition methods, cell structure, and device parameters are reported.

Deposition approach	Cell Structure	V _{oc} (V)	J _{sc} (mA/cm ²)	FF (%)	PCE (%)	Ref
Sequential deposition	ITO/2T-NATA/MAPbI ₃ /C60/BCP/Ag	1.06	22.42	80.9	19.23	¹
	ITO/PTAA/CsPbI ₃ /PCBM/Al	1	15.5	66.0	10.2	²
	ITO/PTAA/MAPbI ₃ /C60/BCP/Agc	1.09	23.11	77.0	19.4	³
Co-deposition	ITO/TaTm:F6-TCNNQ/TaTm/MAPbI ₃ /C60/C60:PbI ₃ /Ag	1.14	22.08	80.5	20.3	⁴
	TCO/MoO ₃ /TaTm/MAPbI ₃ /C60/BCP/Ag	1.077	21.7	82.5	19.3	⁵

ITO/NiO _X /MAPbI ₃ /C60/BCP/(Cu or Au)	1.03	20.6	79.0	16.8	6
ITO/MeO-2PACz/MAPbI ₃ /C60/BCP/Cu	1.15	22.43	79.6	20.5	7
ITO/PTAA/FA _{1-y} CsyPb(I _{1-x} Cl _x) ₃ /C60/BCP/Ag	1.06	23	79.0	19.3	8
ITO/CuPc/FA _{0.83} Cs _{0.17} PbI ₃ /C60/BCP/Au	0.93	21.1	72.0	13.9	9

Table S5 The photovoltaic parameters and hysteresis index for the PSCs shown in **Figure 4a-c**.

Cell area (cm ²)	V _{oc} (V)	J _{sc} (mA/cm ²)	FF (%)	PCE (%)	Hysteresis index
0.09_Frontward	1.001	23.75	78.50	18.56	
0.09_Reverse	0.999	22.95	76.74	17.60	-0.05
0.36_Frontward	1.07	23.34	68.32	17.06	
0.36_Reverse	1.07	22.75	67.14	16.35	-0.04

Reference

- (1) Lei, T.; Li, F.; Zhu, X.; Dong, H.; Niu, Z.; Ye, S.; Zhao, W.; Xi, J.; Jiao, B.; Ding, L.; et al. Flexible Perovskite Solar Modules with Functional Layers Fully Vacuum Deposited. *Solar RRL* **2020**, *4* (11). DOI: 10.1002/solr.202000292.
- (2) Kottokkaran, R.; Gaonkar, H. A.; Bagheri, B.; Dalal, V. L. Efficient p-i-n inorganic CsPbI₃ perovskite solar cell deposited using layer-by-layer vacuum deposition. *Journal of Vacuum Science & Technology A: Vacuum, Surfaces, and Films* **2018**, *36* (4). DOI: 10.1116/1.5029253.
- (3) Tavakoli, M. M.; Tavakoli, R. All-Vacuum-Processing for Fabrication of Efficient, Large-Scale, and Flexible Inverted Perovskite Solar Cells. *physica status solidi (RRL) – Rapid Research Letters* **2020**, *15* (1). DOI: 10.1002/pssr.202000449.
- (4) Momblona, C.; Gil-Escríg, L.; Bandiello, E.; Hutter, E. M.; Sessolo, M.; Lederer, K.; Blochwitz-Nimoth, J.; Bolink, H. J. Efficient vacuum deposited p-i-n and n-i-p perovskite solar cells employing doped charge transport layers. *Energy Environ. Sci.* **2016**, *9* (11), 3456-3463. DOI: 10.1039/c6ee02100j.
- (5) Pérez-del-Rey, D.; Gil-Escríg, L.; Zanoni, K. P. S.; Dreessen, C.; Sessolo, M.; Boix, P. P.; Bolink, H. J. Molecular Passivation of MoO₃: Band Alignment and Protection of Charge Transport Layers in Vacuum-Deposited Perovskite Solar Cells. *Chemistry of Materials* **2019**, *31* (17), 6945-6949. DOI: 10.1021/acs.chemmater.9b01396.
- (6) Abzieher, T.; Schwenzer, J. A.; Moghadamzadeh, S.; Sutterluti, F.; Hossain, I. M.; Pfau, M.; Lotter, E.; Hetterich, M.; Richards, B. S.; Lemmer, U.; et al. Efficient All-Evaporated pin-Perovskite Solar Cells: A Promising Approach Toward Industrial Large-Scale Fabrication. *IEEE Journal of Photovoltaics* **2019**, *9* (5), 1249-1257. DOI: 10.1109/jphotov.2019.2920727.
- (7) Ross, M.; Gil-Escríg, L.; Al-Ashouri, A.; Tockhorn, P.; Jost, M.; Rech, B.; Albrecht, S. Co-Evaporated p-i-n Perovskite Solar Cells beyond 20% Efficiency: Impact of Substrate Temperature and Hole-Transport Layer. *ACS Appl Mater Interfaces* **2020**, *12* (35), 39261-39272. DOI: 10.1021/acsami.0c10898
- (8) Chiang, Y. H.; Anaya, M.; Stranks, S. D. Multisource Vacuum Deposition of Methylammonium-Free Perovskite Solar Cells. *ACS Energy Lett* **2020**, *5* (8), 2498-2504. DOI: 10.1021/acsenergylett.0c00839
- (9) Yuan, Q.; Lohmann, K. B.; Oliver, R. D. J.; Ramadan, A. J.; Yan, S.; Ball, J. M.; Christoforo, M. G.; Noel, N. K.; Snaith, H. J.; Herz, L. M.; et al. Thermally Stable Perovskite Solar Cells by All-Vacuum Deposition. *ACS Appl Mater Interfaces* **2023**, *15* (1), 772-781. DOI: 10.1021/acsami.2c14658

